Seismic failure modes and seismic safety of Hardfill dam

Kun XIONG*[1, 2], Yong-hong WENG[1, 2], Yun-long HE[3, 4]

1. Changjiang Institute of Survey, Planning, Design and Research, Wuhan 430010, P. R. China
2. National Dam Safety Research Center, Wuhan 430010, P. R. China
3. State Key Laboratory of Water Resources and Hydropower Engineering Science,
Wuhan University, Wuhan 430072, P. R. China
4. State Key Laboratory of Hydraulics and Mountain River Engineering,
Sichuan University, Chengdu 610065, P. R. China

Abstract: Based on microscopic damage theory and the finite element method, and using the Weibull distribution to characterize the random distribution of the mechanical properties of materials, the seismic response of a typical Hardfill dam was analyzed through numerical simulation during the earthquakes with intensities of 8 degrees and even greater. The seismic failure modes and failure mechanism of the dam were explored as well. Numerical results show that the Hardfill dam remains at a low stress level and undamaged or slightly damaged during an earthquake with an intensity of 8 degrees. During overload earthquakes, tensile cracks occur at the dam surfaces and extend to inside the dam body, and the upstream dam body experiences more serious damage than the downstream dam body. Therefore, under the seismic conditions, the failure pattern of the Hardfill dam is the tensile fracture of the upstream regions and the dam toe. Compared with traditional gravity dams, Hardfill dams have better seismic performance and greater seismic safety.

Key words: *Hardfill dam; seismic failure mode; seismic safety; microscopic damage model*

1 Introduction

A Hardfill dam is a new type of dam, which has a symmetrical trapezoid cross-section and an impervious concrete face or other impervious facilities on the upstream surface. The dam is filled up with cemented sand-gravel material called Hardfill, which is inexpensive and of low strength. Hardfill material is produced by adding water and a small quantity of cement into riverbed sand and gravel or excavation waste, which can be easily obtained from a nearby dam site. This type of dam is recommended for the advantages of its high degree of safety, its high anti-seismic performance, and its low requirements for the foundation. Besides, dam construction is simple, rapid, and low-cost, and has little negative impact on the environment

——————————————————

(Londe and Lino 1992; Peng et al. 2008). From the 1990s on, the design concept and construction technique of this new type of dam have been put into practice around the world. The first groups of Hardfill dams were built in Greece, Dominica, and France (Coumoulos and Koryalos 2003; Batmaz 2003). The 44-m high Can-Asuja Dam was built in the Philippines (Mason et al. 2008). The Cindere Dam (Batmaz 2003) and Oyuk Dam (Batmaz et al. 2003) in Turkey stand at the heights of 100 m and 107 m, respectively. Moreover, Japanese dam engineers have developed a new dam construction technology using cemented sand and gravel (CSG) (Hirose et al. 2003) and applied it to more than ten temporary or permanent hydraulic structures.

Hardfill dam construction in China dates from 2004. Typical structures include the upstream CSG cofferdam of the Daotang Reservoir (Yang et al. 2007) in Guizhou Province, the downstream CSG cofferdam of the Jiemian Hydropower Station, the upstream CSG cofferdam of the Hongkou Dam (Jia et al. 2006; Yang 2007) in Fujian Province, and the downstream CSG cofferdam of the Shatuo Hydropower Station (Wei et al. 2010) in Guizhou Province.

In a traditional gravity dam, during strong earthquakes, stress concentration usually appears at the dam heel, toe, and neck, causing the dam body a risk of cracking and threatening dam safety. In view of structural dynamics, Hardfill dams, with a symmetrical trapezoidal cross-section, have better structural dynamic stability than gravity dams, which are designed to have triangle cross-sections and nearly vertical upstream surfaces. Therefore, a Hardfill dam has a greater level of seismic safety. Current studies on seismic characteristics and responses of Hardfill dams usually focus on structural analysis. Few focus on seismic damage features and failure modes of Hardfill dams and gravity dams. Thus, it is necessary to further explore seismic behaviors of Hardfill dams.

In the process of producing Hardfill material, the rough productive technique makes the material discrete and inhomogeneous. Micro-cracks and even macroscopic defects exist within the material. The evolutionary process of macroscopic mechanical properties under the external load acting on micro-cracks existing in the material can be simulated with a numerical method based on the damage mechanics theory. Tang and Zhu (2003) and Zhu and Tang (2002) studied the fracture process of the rock using a model with the Weibull distribution to characterize the random distribution of the mechanical properties of materials. This study adopted this approach and used the random distribution function to reflect the influence of the inhomogeneity of Hardfill material. In the simulation of the dam with the finite element method (FEM), each element was considered a continuous media, but the mechanical properties, such as the elastic modulus, strength, and Poisson's ratio, were different for different elements. The FEM model can be regarded as a sample space where each element is a sample point. When the number of elements is large enough, owing to having enough sample points, mechanical properties of the damming material can be considered stochastic variables, which obey certain random distribution rules. The sample means stand for the general levels of

the material's properties and the variances represent the discrete degree. Although microscopic structures such as aggregates and mortar contained in each single element cannot be described accurately with this method, the influence of the inhomogeneity of Hardfill material can be reflected to some extent, which makes the computation results more actual.

Based on microscopic damage theory and the finite element method, and utilizing the Weibull distribution to characterize the random distribution of the mechanical properties of materials, the microscopic damage model was set up in this study to reflect the influence of inhomogeneity of Hardfill material. The seismic response of a typical Hardfill dam was analyzed during strong earthquakes with intensities of 8 degrees and even greater. A gravity dam with the same height was analyzed for comparison. Different seismic damage features and failure modes of the Hardfill dam and gravity dam during earthquakes were examined and the seismic failure mechanism of dams was explored as well.

2 Microscopic damage model for inhomogeneous material

2.1 Characterization of material inhomogeneity

The elastic modulus and strength parameters were considered to be stochastic variables in this study, and they are supposed to obey the Weibull distribution. After discretizing test specimens or dam structures with the finite element mesh, material parameter values were assigned to each element randomly, and then the test specimens or dam structures became inhomogeneous. It needs to be pointed out that inhomogeneous materials with different degrees of inhomogeneity can be acquired using different Weibull distribution parameters, and, even following the same Weibull distribution, the space distribution of material parameters of the entire structure also diversify as each material parameter value is produced randomly. The density function of the Weibull distribution is

$$f(x) = \frac{m}{x_0} \left(\frac{x}{x_0} \right)^{m-1} e^{-\left(\frac{x}{x_0} \right)^m} \qquad x > 0 \qquad (1)$$

where x is the material parameter that obeys the Weibull distribution, x_0 is a parameter related to the mean of material parameter values, and m is the shape parameter of the density function curve of Weibull distribution. The parameter m reflects the discrete degree of material parameters. When m changes from a low value to a high value, the density function curve changes its shape from low and wide to high and narrow, which demonstrates that the material parameter x is closer to x_0. Hence, the shape parameter m is called the homogeneity coefficient in this study. The higher the m value is, the more homogeneous the material is, and the lower the variance of the density function is.

2.2 Damage constitutive relationship for microscopic elements

The continuum damage constitutive model was adopted for each single microscopic

element, while the random distribution function was used for the entire dam to reflect macro-inhomogeneity of material mechanical parameters. With an adequate element mesh density, a simple constitutive model could be applied in the analysis. Furthermore, the anisotropic damage could be ignored and the impact of element size on fracture energy was limited, due to the fine element mesh, which made the calculation more convenient (Tang and Zhu 2003). The constitutive equation for each microscopic element under the uniaxial stress state can be expressed as

$$\sigma = E_0 (1-D)\varepsilon \tag{2}$$

where σ is the stress, ε is the strain, D is a damage variable, and E_0 is the initial elastic modulus, namely the elastic modulus in an undamaged state.

Each microscopic element is elastic initially, and its stress increases with the load. When its stress or strain approaches a critical value determined by damage criteria, the element begins to be damaged or even destroyed. Two damage criteria were considered: the maximum tensile strain criterion and Mohr-Coulomb criterion. When the maximum principal tensile strain reaches the tensile strain corresponding to the tensile strength, tensile damage occurs in the material. Once the maximum principal tensile strain reaches the ultimate tensile strain value, the microscopic elements are completely destroyed, which means that a macroscopic crack appears. Then, the cracking element is given a small elastic modulus value for calculation. In the calculation process, the strain state of each microscopic element is judged by the maximum tensile strain criterion first. If the maximum tensile strain criterion is met, the Mohr-Coulomb criterion is not adopted. When the element is in a compressive or shear state, the Mohr-Coulomb criterion is used to determine whether shear failure occurs. The Mohr-Coulomb criterion can be converted into

$$F = \frac{1+\sin\varphi}{1-\sin\varphi}\sigma_1 - \sigma_3 \geq f_c \tag{3}$$

where F is the yield function, σ_1 is the first principal stress, σ_3 is the third principal stress, φ is the internal friction angle, and f_c is the uniaxial compressive strength.

Fig. 1 shows the microscopic tensile and shear (compress) damage constitutive relationships of Hardfill material adopted in this study. Positive values stand for tensile stress or tensile strain. In Fig. 1, σ_t and σ_c are the tensile and compressive stresses, respectively, ε_t and ε_c are the tensile and compressive strains, respectively, f_{t0} and f_{c0} are the uniaxial tensile and compressive strengths, respectively, ε_{t0} is the tensile strain corresponding to the tensile strength, ε_{c0} is the compressive strain corresponding to the compressive strength, ε_{tu} and ε_{cu} are the ultimate tensile and compressive strains, respectively, f_{cr} is the residual strength, ε_{cr} is the compressive strain corresponding to the residual strength, ξ is the ultimate tensile strain coefficient, λ is the residual strength coefficient, r is the residual strain coefficient, and ζ is the ultimate compressive strain coefficient.

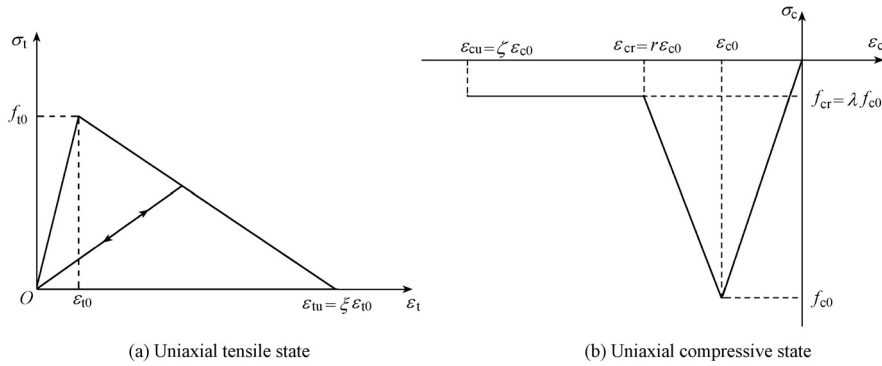(a) Uniaxial tensile state   (b) Uniaxial compressive state

Fig. 1 Microscopic damage constitutive relationships of Hardfill material

Under the uniaxial tensile condition, the damage variable D_t, which is used to replace D in Eq. (2), can be expressed as

$$D_t = \begin{cases} 0 & 0 \leq \varepsilon_t \leq \varepsilon_{t0} \\ 1 - \left(\dfrac{\xi}{\xi-1} \dfrac{\varepsilon_{t0}}{\varepsilon_t} - \dfrac{1}{\xi-1} \right) & \varepsilon_{t0} \leq \varepsilon_t \leq \varepsilon_{tu} \\ 1 & \varepsilon_t > \varepsilon_{tu} \end{cases} \tag{4}$$

When the tensile strain ε_t reaches ε_{t0}, the element enters the damage stage. When ε_t reaches the ultimate tensile strain ε_{tu}, complete damage occurs, and then the damage variable D_t is equal to 1.

In the triaxial stress state, damage is still considered to be isotropic. When the tensile strain of the element meets the maximum tensile strain criterion, the one-dimensional damage constitutive model expands to the three-dimensional model according to the method developed by Mazars (1984). The equivalent strain $\bar{\varepsilon}$ is used to replace ε and can be expressed as

$$\bar{\varepsilon} = \sqrt{\varepsilon_1^2 + \varepsilon_2^2 + \varepsilon_3^2} \tag{5}$$

where ε_1, ε_2, and ε_3 are the first, second, and third principal strains, respectively. Each principal strain is taken as zero when smaller than zero.

Under the uniaxial compressive condition, the damage variable D_c, which is used to replace D in Eq. (2), can be expressed as

$$D_c = \begin{cases} 0 & \varepsilon_{c0} \leq \varepsilon_c \leq 0 \\ 1 - \left(\dfrac{\zeta-\lambda}{\zeta-1} \dfrac{\varepsilon_{c0}}{\varepsilon_c} - \dfrac{\lambda-1}{\zeta-1} \right) & \varepsilon_{cr} \leq \varepsilon_c < \varepsilon_{c0} \\ 1 - \dfrac{\lambda\varepsilon_{c0}}{\varepsilon_c} & \varepsilon_{cu} \leq \varepsilon_c < \varepsilon_{cr} \\ 1 - \dfrac{\lambda}{\zeta} & \varepsilon_c < \varepsilon_{cu} \end{cases} \tag{6}$$

When the compressive strain ε_c of the element reaches ε_{c0}, compressive damage occurs. When ε_c reaches the ultimate compressive strain ε_{cu}, complete damage occurs, and then D_c is equal to a fixed value.

When the element is under multi-axial stress conditions and the stress meets the Mohr-Coulomb criterion, the maximum compressive principal strain ε_{cmax} is used to replace the uniaxial stain ε_{c0} in Eq. (6) to make damage judgments. The maximum compressive principal strain ε_{cmax} can be expressed as

$$\varepsilon_{cmax} = \frac{1}{E_0}\left[-f_c + \frac{1+\sin\varphi}{1-\sin\varphi}\sigma_1 - \mu(\sigma_1 + \sigma_2)\right] \tag{7}$$

where μ is Poisson's ratio.

2.3 Model parameters

Plane stress numerical specimens under the uniaxial tensile condition were set up, and five microscopic material parameter samples with the same macroscopic material parameters and homogeneity coefficient m ($m = 1.5$) were generated. Fig. 2 and Fig. 3 show fracture patterns and stress-strain relationships of the specimens with different random materials under the uniaxial tensile condition, respectively. Calculation results show that randomness of the material's microscopic structure induces random macroscopic fracture patterns of the specimen. However, failure modes of specimens remain the same and the randomness of material parameters has little influence on the macroscopic elastic modulus and strength obtained through numerical tests. The macroscopic stress-strain curves of five samples are almost coincident in the elastic and nonlinear stages, and a certain difference exists just in the softening stage.
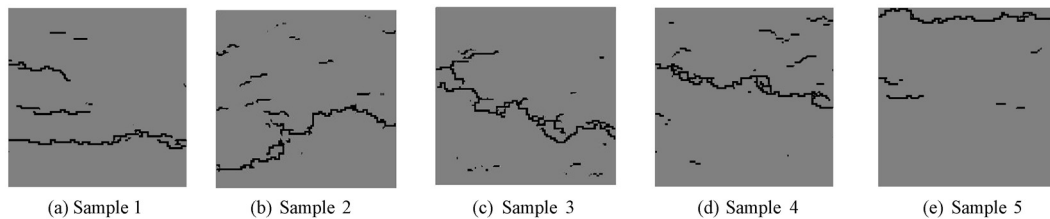

(a) Sample 1　　(b) Sample 2　　(c) Sample 3　　(d) Sample 4　　(e) Sample 5

Fig. 2 Fracture patterns of Hardfill specimens with different random material samples under uniaxial tensile condition
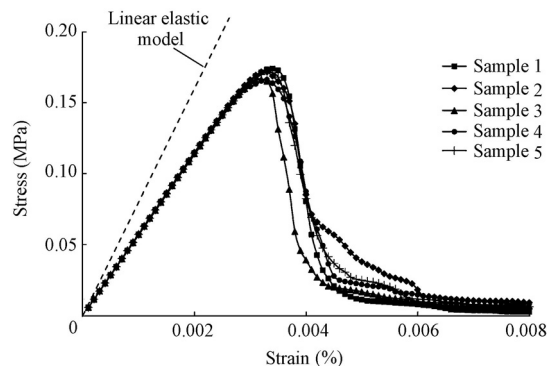

Fig. 3 Stress-strain relationship of Hardfill specimens with different random material samples under uniaxial tensile condition

In order to study the influence of the microscopic degree of inhomogeneity of material on macroscopic characteristics, the value of the parameter m was set as 1, 1.5, 2, 3, 5, and 10, respectively. Fig. 4 and Fig. 5 show fracture patterns and stress-strain relationships of the specimens with different homogeneity coefficients under the uniaxial tensile condition, respectively. Along with the increase of the homogeneity coefficient m, differences of the material's property parameter values between different microscopic elements decrease, but macroscopic cracks of the uniaxial tensile specimens with different homogeneity coefficients show little difference. One obvious change is that, given the same values for other microscopic parameters, the macroscopic elastic modulus and strength increase gradually as the homogeneity coefficient increases. In other words, the difference between macroscopic and microscope characteristics gets smaller when the material is more homogeneous. In addition, the brittleness of material is more apparent with the increase of the homogeneity coefficient.
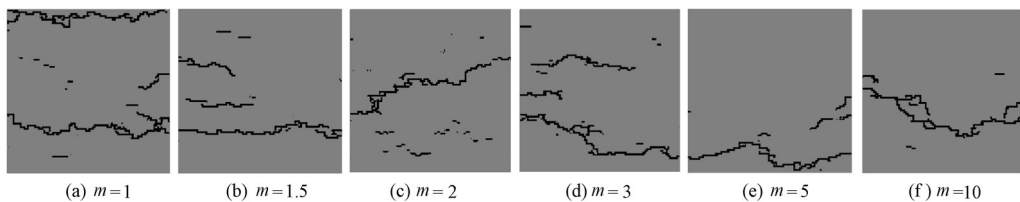

(a) $m=1$ (b) $m=1.5$ (c) $m=2$ (d) $m=3$ (e) $m=5$ (f) $m=10$

Fig. 4 Fracture patterns of Hardfill specimens with different homogeneity coefficients under uniaxial tensile condition
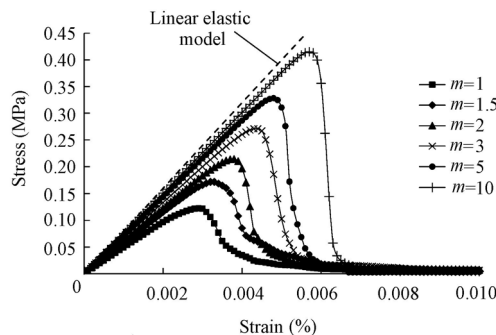

Fig. 5 Stress-strain relationship of Hardfill specimens with different homogeneity coefficients under uniaxial tensile condition

Fig. 6 shows the relationship between the ratio of the microscopic elastic modulus (E_{mic}) to the macroscopic elastic modulus E_{mac} and the homogeneity coefficient, and the relationship between the ratio of the microscopic strength (f_{mic}) to the macroscopic strength f_{mac} and the homogeneity coefficient based on uniaxial tensile numerical calculation. They fit logarithm function curves. This conclusion can be acquired by uniaxial compressive numerical analysis as well.

The ultimate tensile strain coefficient of Hardfill material in this study was fixed at 8. As can be seen from the stress-strain curves with $m = 5$ and 10 shown in Fig. 5, the macroscopic constitutive relationships still show obvious brittleness even if the constitutive relationships of

microscopic elements have a certain ductility. This is because the decrease of the specimen's macroscopic strength depends on whether a large amount of microscopic elements are damaged simultaneously, which is decided by the homogeneity coefficient. Thus, this also illustrates that the homogeneity coefficient is a critical factor and the softening form of the stress-strain relationship of the microscopic elements has little influence on the macroscopic response of specimens.
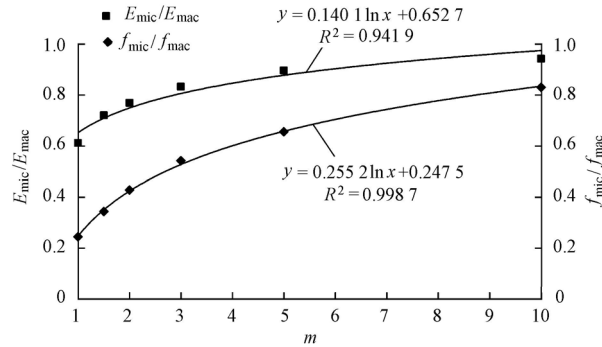

Fig. 6 Relationship between ratio of microscopic parameter to macroscopic parameter and homogeneity coefficient

3 Seismic analysis of Hardfill dam with microscopic damage model

3.1 Numerical model

Fig. 7 shows the profile of a typical Hardfill dam. The height of the Hardfill dam is 70 m and the dam crest is 10 m wide. The upstream and downstream dam slope ratios are both 1:0.7, like those of the Cindere Dam and Oyuk Dam. The interface between the dam body and foundation and generalized construction joint surfaces within the dam body are simulated with the FEM model. The element size of the FEM mesh is 0.5 m × 0.5 m, and the calculation domain of the FEM model is extended by 1.5 times the height of the dam upstream and downstream foundation in the horizontal direction, and one time that in the vertical direction. Fig. 8(a) shows the FEM mesh of the Hardfill dam. A comparative analysis was made between the Hardfill dam and the traditional gravity dam. Both dams have the same height, downstream slope ratio (1:0.7), and foundation condition. The two dams also have the same element size of the FEM mesh. The FEM mesh of the gravity dam is shown in Fig. 8(b).
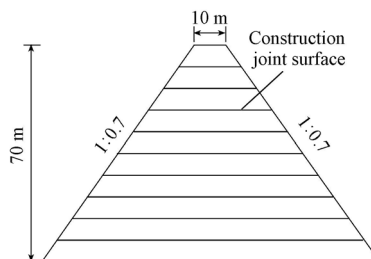

Fig. 7 Hardfill dam profile
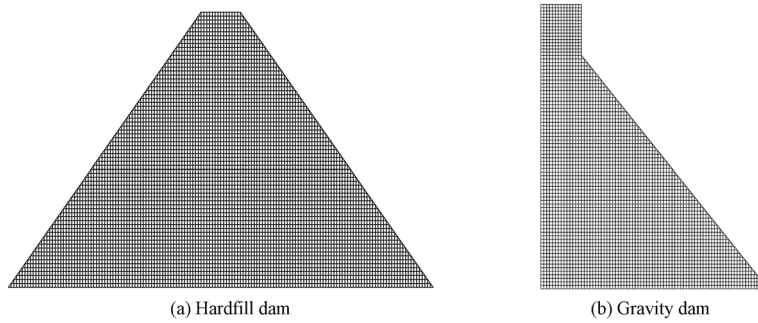
(a) Hardfill dam   (b) Gravity dam

Fig. 8 FEM meshes of dams

In static analysis, main loads included the deadweight of the dam, the water pressure on the upstream face, and the uplift pressure on the dam foundation. The upstream and downstream water levels were 70 m and 0 m, respectively. The uplift water head was assumed to be 1/2 of the upstream water head at the dam heel and 0 at the dam toe, following linear distribution along the foundation surface. The time-history method was used here for seismic analysis and the Taft earthquake waves were chosen as the input ground motion, as shown in Fig. 9 and Fig. 10. The earthquake duration for the calculation was 12 seconds and the time step was 0.02 seconds. The maximum value of acceleration was adjusted to $0.2g$ and the dominant period to 0.2 seconds. The transverse and vertical motions were input simultaneously, but the vertical peak acceleration was 2/3 the transverse peak acceleration. In order to eliminate the amplifying effect of the foundation, the mass of the foundation was ignored. The loads considered in the seismic calculation included the deadweight of the dam,
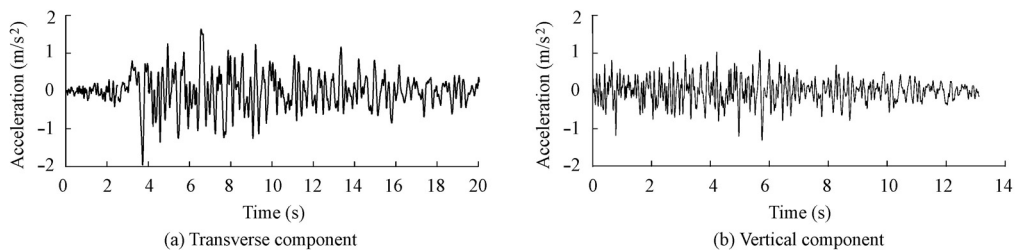

(a) Transverse component   (b) Vertical component

Fig. 9 Input earthquake ground motion

(a) Transverse acceleration response spectrum   (b) Vertical acceleration response spectrum
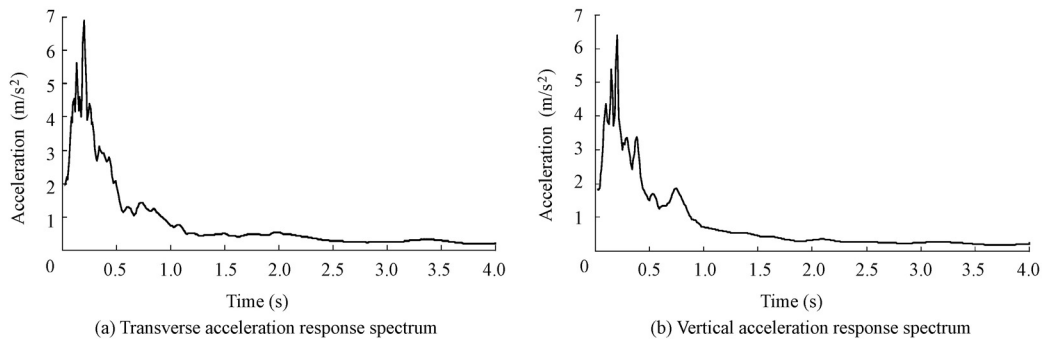
Fig. 10 Acceleration response spectrum of input earthquake ground motion

water pressure, and seismic loads. The effect of hydrodynamic pressure was taken into account as the added mass matrix, which was calculated by the Westergaard formula.

The property parameters of materials are listed in Table 1. The means of the microscopic elastic modulus and compressive strength were obtained according to the curves in Fig. 6. The distributions of the microscopic elastic modulus and compressive strength are shown in Fig. 11. The elastic modulus and strength in seismic analysis were 1.3 times those in static analysis, while Poisson's ratio did not change. The damping ratio was set to be 0.05 and Rayleigh damping was used.

Table 1 Property parameters of materials for static analysis

Material	ρ (kg/m^3)	m	μ	φ (°)	E_{mac} (GPa)	E_{mic} (GPa)	f_{tmac} (MPa)	f_{tmic} (MPa)	f_{cmac} (MPa)	f_{cmic} (MPa)
Hardfill	2 300	1.5	0.2	40	8.0	11.11	0.50	1.45	5.0	14.53
Dam-foundation interface	2 300	1.5	0.2	30	8.0	11.11	0.40	1.12	4.0	11.63
Construction joint surface	2 300	1.5	0.2	30	8.0	11.11	0.40	1.12	4.0	11.63
Concrete	2 400	3.0	0.167	50	25.5	30.68	1.54	2.38	13.4	20.68
Foundation	2 500	3.0	0.25	50	15.0	18.05	1.00	1.54	10.0	15.43

Note: ρ is the density of materials, f_{tmac} and f_{tmic} are the macroscopic and microscopic tensile strengths, respectively, and f_{cmac} and f_{cmic} are the macroscopic and microscopic compressive strengths, respectively.

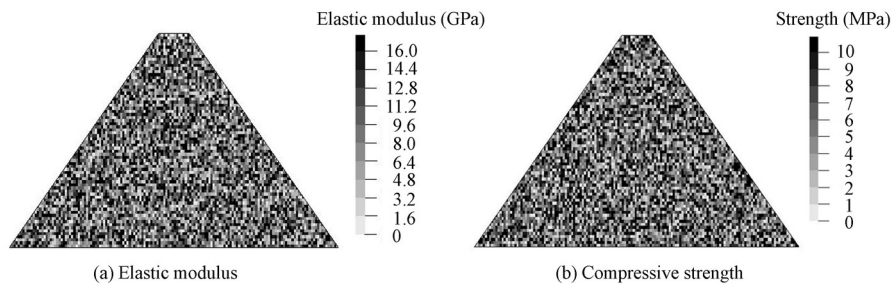(a) Elastic modulus   (b) Compressive strength

Fig. 11 Distributions of microscopic elastic modulus and compressive strength of Hardfill dam

The homogeneity coefficient should be chosen on the basis of statistical analysis of experimental results in actual projects, but in the absence of statistical data, assumed values judged from material inhomogeneity conditions are often used. According to numerical experiments carried out by Tang and Zhu (2003), in microscopic analysis of concrete, the homogeneity coefficient is usually 6.0 for aggregates, 3.0 for mortar, and 1.5 for interfaces between aggregates and mortar. After selecting the homogeneity coefficient of Weibull distribution and constitutive relationships for microscopic elements, numerical specimens under typical stress conditions should be set up to check whether the specimens created by chosen parameters have the same macroscopic mechanical properties as the real one. If not, previously chosen parameters need to be adjusted until the specimens can reflect real macroscopic mechanical characteristics.

3.2 Dynamic response of Hardfill dam under earthquake with intensity of 8 degrees

The dynamic properties of the Hardfill dam can be acquired from Xiong et al. (2007). The dynamic response of the Hardfill dam during an earthquake with an intensity of 8 degrees is shown in Fig. 12. A positive stress value stands for a tensile stress and a negative stress value stands for a compressive stress. During an earthquake with an intensity of 8 degrees, the dynamic responses of the Hardfill dam simulated with a microscopic damage model generally comply with the results obtained from a linear elastic model (Fig. 13), especially the distribution of acceleration and displacement, whose maximum values both appear on the dam crest. This demonstrates that the microscopic damage constitutive model can be applied to static and dynamic analyses of the Hardfill dam. However, when using this model, the stress isolines are not very smooth because of the material inhomogeneity.

Figs. 12(c) and (d) clearly show the influence of material inhomogeneity on the stress distribution inside the dam. The stress distribution inside the dam appears to be inhomogeneous, and stress values of different microscopic elements show a lot of variation. Generally, the tensile stress appears at the dam heel and nearby downstream dam surface, but the value is small. Large principal compressive stress appears near the dam heel, dam toe, and dam surfaces. These results are coincident with the stress distribution characteristics obtained from the linear elastic model (Fig. 13). The analysis results indicate that the Hardfill dam remains at a low stress level, undamaged or slightly damaged, during the earthquake with an intensity of 8 degrees.
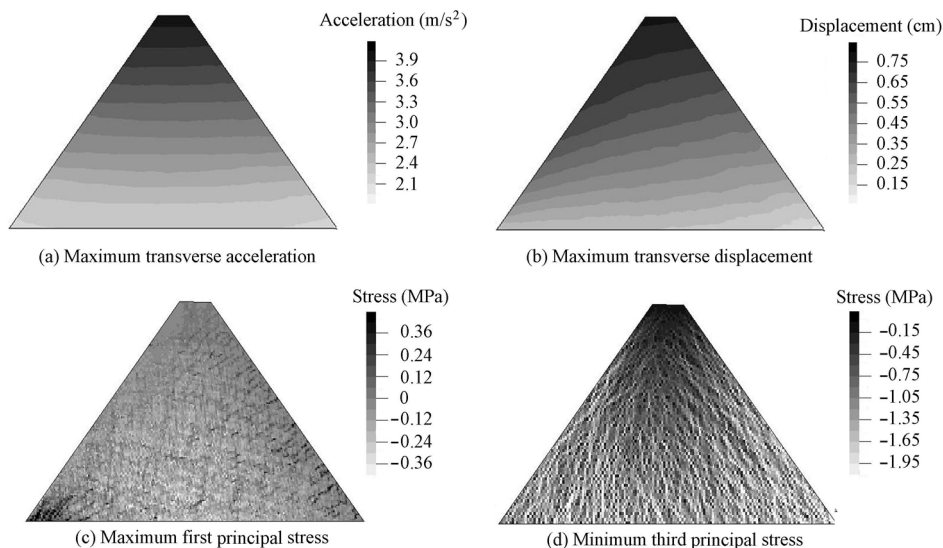

(a) Maximum transverse acceleration

(b) Maximum transverse displacement

(c) Maximum first principal stress

(d) Minimum third principal stress

Fig. 12 Dynamic response of Hardfill dam simulated with microscopic damage model during earthquake with intensity of 8 degrees

(a) Maximum transverse acceleration

(b) Maximum transverse displacement

(c) Maximum first principal stress

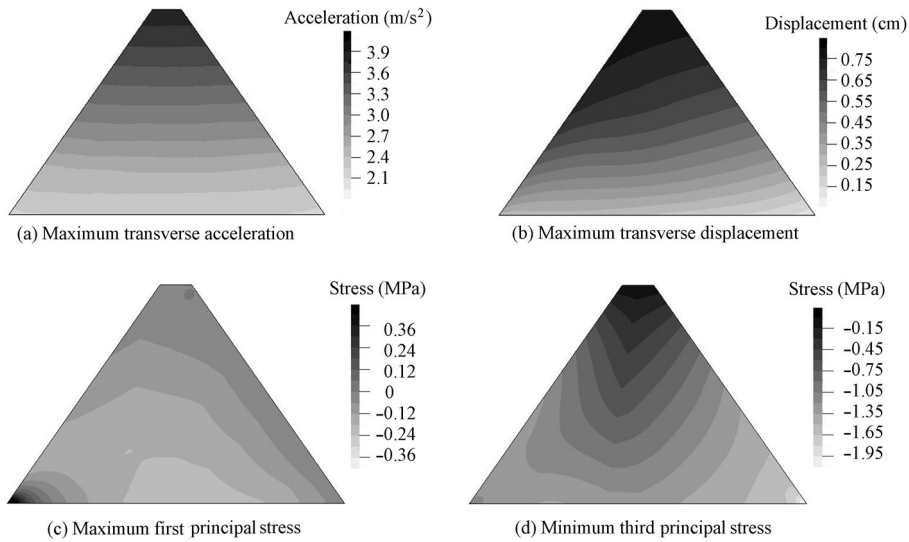(d) Minimum third principal stress

Fig. 13 Dynamic response of Hardfill dam simulated with linear elastic model during earthquake with intensity of 8 degrees

3.3 Seismic failure modes of dam under overload earthquakes

Based on the static analysis, dam stress distribution and structural damage in a dynamic situation were analyzed through the earthquake acceleration overload method. The amplitudes of overload earthquakes were amplified and scaled to different peak accelerations. The microscopic damage model and linear elastic model were both used in the calculation. Fig. 14 and Fig. 15 show the maximum first principal stress distributions of the gravity dam and Hardfill dam during the earthquakes with different peak accelerations, obtained using the linear elastic model. During the earthquakes, maximum first principal tensile stresses appeared at the dam heel, upstream, and downstream surfaces of the gravity dam, and stress concentrated at the dam heel. When the earthquake intensity grew, the maximum first principal tensile stress increased rapidly, indicating that cracks tended to appear. For the Hardfill dam, the maximum first principal tensile stresses appeared at the upstream and downstream surfaces, and the dam heel and toe were the stress concentration areas that could be damaged in strong earthquakes.
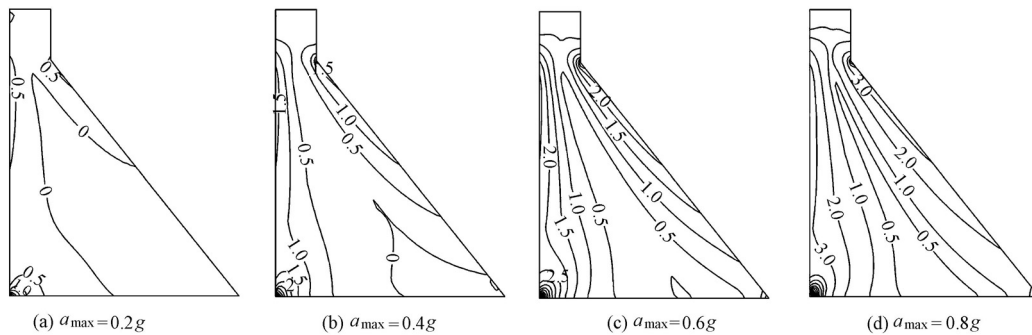

(a) $a_{max} = 0.2g$ (b) $a_{max} = 0.4g$ (c) $a_{max} = 0.6g$ (d) $a_{max} = 0.8g$

Fig. 14 Maximum first principal stress of gravity dam simulated with linear elastic model during earthquakes with different peak accelerations a_{max} (Unit: MPa)
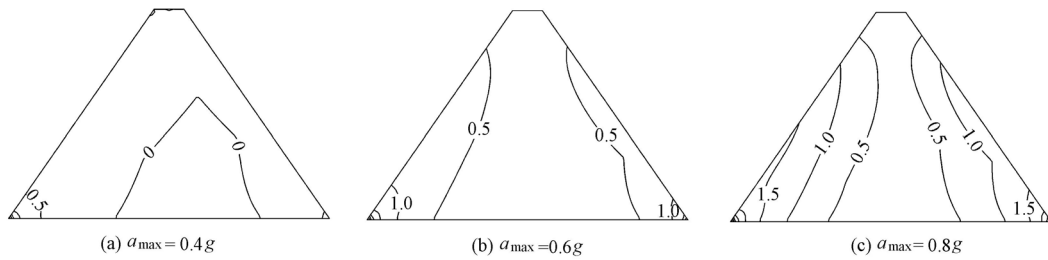
Fig. 15 Maximum first principal stress of Hardfill dam simulated with linear elastic model during earthquakes with different peak accelerations a_{max} (Unit: MPa)

Fig. 16 and Fig. 17 show the failure modes of the Hardfill dam and gravity dam during earthquakes with different peak accelerations, obtained using the microscopic damage model. The black areas are macroscopic cracks.
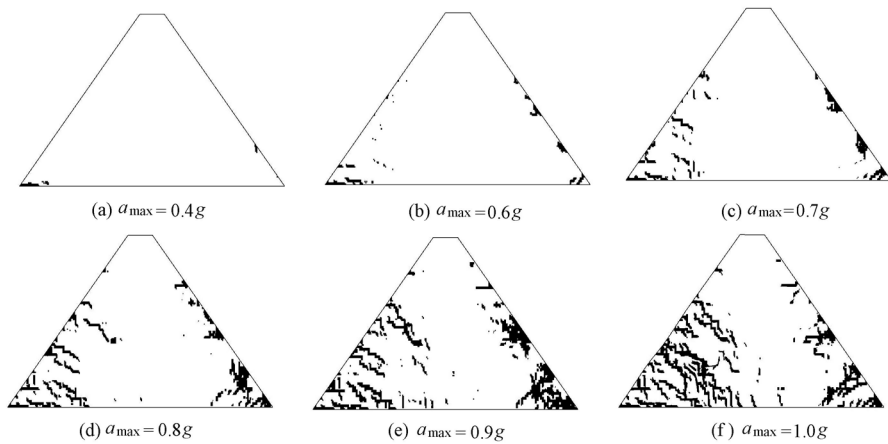

Fig. 16 Seismic failure modes of Hardfill dam simulated with microscopic damage model during earthquakes with different peak accelerations a_{max}
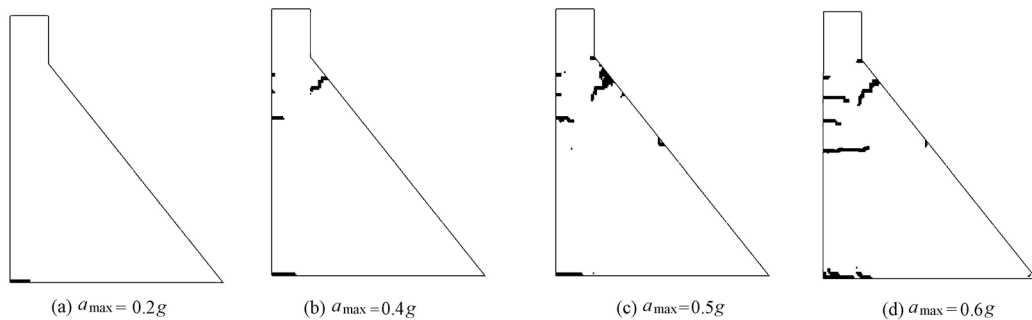

Fig. 17 Seismic failure modes of gravity dam simulated with microscopic damage model during earthquakes with different peak accelerations a_{max}

The Hardfill dam has few damage areas during the earthquake with an intensity of 8 degrees. It can be seen from Fig. 16 that during a 9-degree earthquake with a peak acceleration of 0.4g, only an area at the interface between the dam body and foundation near the dam heel is obviously damaged, and cracks appear at the downstream dam surface. With the increase of the earthquake peak acceleration, cracks along the interface between the dam body and

foundation near the dam heel extend downstream, and cracks near the dam toe arrive at the dam foundation. Regional cracks perpendicular to both upstream and downstream dam surfaces appear in the dam body, and there are more cracks in the upstream dam body than the downstream body. These regional cracks usually emerge at the construction joint surfaces, but do not extend along these joint surfaces. When the earthquake intensity increases dramatically, the cracks emerging from dam surfaces gradually connect with the regional cracks and then extend to the dam foundation, forming the final seismic damage pattern of the Hardfill dam. The dam crest experiences permanent horizontal deformation, which can be seen in Fig. 18(a).

As for a typical gravity dam, a few cracks appear at the dam heel during the earthquake with an intensity of 8 degrees. With an increase of peak acceleration, the cracks extend downstream along the interface between the dam body and foundation to a certain depth. Cracks appear at dam surfaces near the dam neck and these cracks perpendicular to the dam surfaces extend toward inside the dam body. At a peak acceleration of 0.6g, damage areas around the dam neck link together and the two macro-cracks on upstream and downstream dam surfaces almost connect. In addition, several horizontal cracks appear on the upstream dam surface. This is the typical seismic damage pattern of the gravity dam. It can be seen from Fig. 18(b) that, because of the dam neck fracture, there is obvious permanent deformation at the dam crest, while permanent deformation beneath the dam neck is not significant.
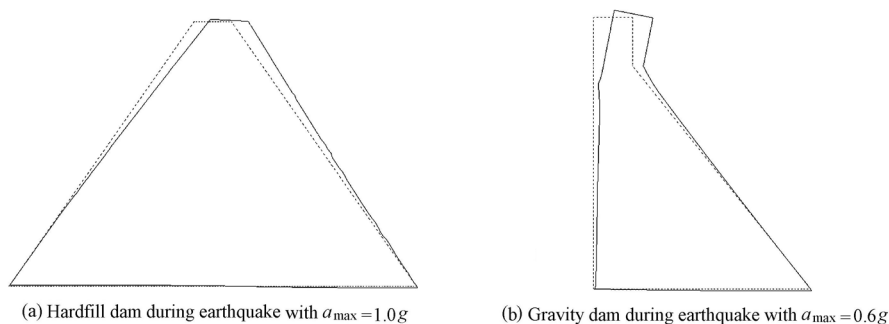

(a) Hardfill dam during earthquake with $a_{max} = 1.0g$ (b) Gravity dam during earthquake with $a_{max} = 0.6g$

Fig. 18 Permanent deformation of dams under earthquakes (deformation enlarged by 200 times)

Compared with a gravity dam, a Hardfill dam has low material strength. However, the fat section causes the Hardfill dam to have better seismic performance. Nevertheless, the Hardfill dam has more cracks, seen from seismic failure patterns obtained with the microscopic damage model (Fig. 16). The reason for this is that the Hardfill dam has more weak gaps, as simulated in the numerical model of the low-strength construction joint surfaces, and the material of the Hardfill dam is more inhomogeneous than that of the gravity dam.

It can be seen from Fig. 16 that a lot of generalized construction joint surfaces have been simulated in the Hardfill dam model, but cracks do not extend along these joint surfaces, because of the strong inhomogeneity of the dam material. Fig. 19 shows different damage modes of the Hardfill dam with different degrees of homogeneity during an earthquake with a peak acceleration of 1.0g. With a larger homogeneity coefficient m, more cracks develop along

the joint surfaces, and regional diffuse cracks decrease. The interface between the dam body and the foundation is the most severely damaged area. Even so, seismic failure modes with different degrees of homogeneity still have common characteristics: dam toes experience similar damage, and cracks emerging on the upstream dam surface, which are perpendicular to the dam surface, extend to the interface between the dam body and the foundation. Therefore, under seismic conditions, the failure pattern of the Hardfill dam is the tensile fracture of the upstream regions and the dam toe.
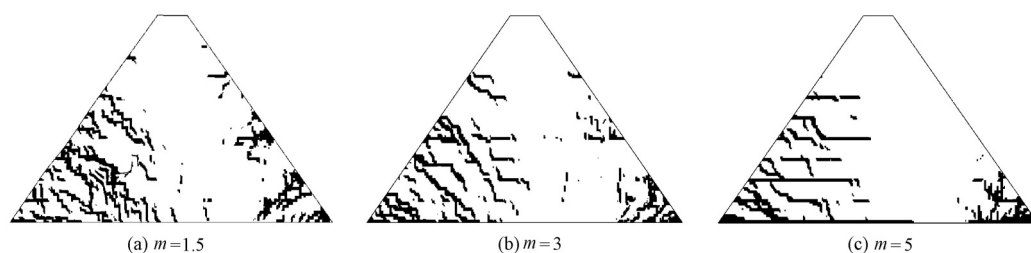

(a) $m = 1.5$ (b) $m = 3$ (c) $m = 5$

Fig. 19 Seismic failure modes of Hardfill dam with different homogeneity coefficients during earthquake with $a_{max} = 1.0g$

4 Conclusions

Based on microscopic damage theory and the finite element method, and using the Weibull distribution to characterize random distribution of the mechanical properties of materials, failure modes and seismic safety of a typical Hardfill dam during earthquakes were studied and analyzed. Conclusions are as follows:

(1) During an earthquake with an intensity of 8 degrees, the seismic responses of the Hardfill dam simulated with a microscopic damage model are generally consistent with those obtained by a linear elastic model. This shows that the microscopic damage constitutive model can be applied to static and dynamic analyses of a Hardfill dam.

(2) A Hardfill dam remains at a low stress level, undamaged or slightly damaged during an earthquake with an intensity of 8 degrees. However, stress values of different microscopic elements show a lot of variation, due to inhomogeneity of the Hardfill material.

(3) During earthquakes, there are damage areas in both the upstream and downstream body of the Hardfill dam because its symmetrical section is under alternating inertial forces. The upstream dam body experiences more serious damage than the downstream dam body. With the increase of the earthquake peak acceleration, tensile cracks occur at dam surfaces and then extend to inside the dam body. Therefore, under seismic conditions, the failure pattern of the Hardfill dam is the tensile fracture of the upstream regions and the dam toe.

(4) Compared with the traditional gravity dam, the trapezoidal Hardfill dam has better seismic performance and greater seismic safety.

References

Batmaz, S. 2003. Cindere dam-107 m high roller compacted hardfill dam (RCHD) in Turkey. Berga, L., Buil, J. M., Jofre, C., and Chonggang, S., eds., *Proceedings of the 4th International Symposium on Roller Compacted Concrete (RCC) Dams*, 121-126. Rotterdam: A.A. Balkema.

Batmaz, S., Köksal, A., Ergeneman, I., and Pekcagliyan, D. 2003. Design of the 100 m-high Oyuk Hardfill dam. *International Journal on Hydropower and Dams*, 10(5), 138-142.

Coumoulos, D. G., and Koryalos, T. P. 2003. Lean RCC dams-laboratory testing methods and quality control procedure during construction. Berga, L., Buil, J. M., Jofre, C., and Chonggang, S., eds., *Proceedingsof the 4th International Symposium on Roller Compacted Concrete Dams*, 233-238. Rotterdam: A.A. Balkema.

Hirose, T., Fujisawa, T., Kawasaki, H., Kondo, M., Hirayama, D., and Sasaki, T. 2003. Design concept of trapezoid-shaped CSG dam. Berga, L., Buil, J. M., Jofre, C., and Chonggang, S., eds., *Proceedings of the 4th International Symposium on Roller Compacted Concrete Dams*, 457-464. Rotterdam: A.A. Balkema.

Jia, J. S., Ma, F. L., Li, X. Y., and Chen, Z. P. 2006. Study on material characteristics of cement-sand-gravel dam and engineering application. *Journal of Hydraulic Engineering*, 37(5), 578-582. (in Chinese).

Londe, P., and Lino, M. 1992. The faced symmetrical hardfill dam: A new concept for RCC. *Water Power and Dam Construction*. 44(2), 19-24.

Mason, P. J., Hughes, R. A. N., and Molyneux, J. D. 2008. The design and construction of a faced symmetrical hardfill dam. *International Journal on Hydropower and Dams*, 15(3), 90-94.

Mazars, J. 1984. *Application de la Mecanique de Lendnnag Emment an Comportememt Non Lineaire de Structure*. Ph. D. Dissertation. Paris: *These de Doctorat Detat Univ*ersity. (in Paris)

Peng, Y. F., He, Y. L., and Wan, B. 2008. Hardfill dam: A new design RCC dam. *Water Power*, 34(2), 61-63, (in Chinese)

Tang, C. A., and Zhu, W. C. 2003. D*amage and Fracture of Concrete*. Beijing: Science Press. (in Chinese)

Wei, J. Z., Wu, Z. T., Wu, Y. W., and Zhu, X. Q. 2010. Study and application of new poor cemented Hardfill construction technology. *Construction Technologies of Chinese Roller Compacted Concrete (RCC) Dams*, 164-171. Beijing: China Water and Power Press. (in Chinese)

Xiong, K., He, Y. L., and Peng, Y. F. 2007. Study on Seismic Safety of Hardfill Dam. *Proceedings of the 5th International Symposium on Roller Compacted Concrete (RCC) Dams*, 877-884. Beijing: China Water and Power Press.

Yang, S. L. 2007. Characteristics and load carrying capacity of CSG dam construction materials. *China Civil Engineering Journal*, 40(2), 97-103. (in Chinese)

Yang, Z. H., Zhao, Q. X., Fu, X. P., Chen, W. M., and Fu, C. S. 2007. Study on CSG dam construction technique and its application to Daotang Reservoir Project. *Water Resources and Hydropower Engineering*, 38(8), 46-49. (in Chinese)

Zhu, W. C., and Tang, C. A. 2002. Numerical simulation on shear fracture process of concrete using mesoscopic mechanical model. *Construction and Building Materials*, 16(8), 453-463. [doi:10.1016/ S0950-0618(02)00096-X]

(Edited by Yan LEI)